Thesis Final Report

Numerical stability of (3+1)D hydrodynamic simulation of relativistic heavy-ion collisions

Guilherme H. Caumo (260964615)

Supervised by Prof. Sangyong Jeon

McGill University, Department of Physics

Abstract

Hydrodynamics presents one of the simplest models for systems involving many-body dynamics and macroscopic physical phenomena. Considering this, studies have applied hydrodynamics to describe extremely hot and dense fluid-like phenomena such as the strongly-coupled quark-gluon plasma (sQGP) that occurs during the hydrodynamic phase of heavy-ion collisions. To further these efforts, the MUScl (Monotonic Upstream-centered Schemes for Conservation Laws) for Ion Collisions (MUSIC) algorithm was developed, initially with ideal hydrodynamics, to study the behavior of sQGP. Thereafter, viscous hydrodynamics were implemented in the algorithm, but the resulting code exhibited numerical instability under certain circumstances. Therefore, the first section for this report will feature a thorough review of the literature concerning relativistic hydrodynamics. Following this, heavy-ion collisions, particularly the sQGP stage, will be examined using hydrodynamic models through the MUSIC algorithm. This report aims to introduce MUSIC's viscous hydrodynamic code and present the instabilities in its numerical scheme. These instabilities are then analyzed with the aim of identifying root causes. The report successfully identifies unphysically large gradients at low-density regions as the underlying cause by demonstrating that unphysically large values for flow velocity, expansion rate, and Navier-Stokes tensor occur at unstable regions.

1 Introduction

1.1 Motivation and Goals

The MUSIC algorithm is a (3+1) dimensional hydrodynamic simulation of relativistic heavy-ion collisions. The current iteration of MUSIC can apply viscous hydrodynamics to the evolution of strongly-coupled quark-gluon plasma (sQGP), however, it experiences numerical instabilities that results in unphysical elements in runs, such as expansions of plasma in regions that should not occur. These instabilities have been mitigated by checking for when these elements occur and eliminating them to prevent the evolution of the sQGP from developing unphysically, one of these regulators is "QuestRevert," but instabilities still occur on a minority of events. Therefore, the motivation behind this project is to study the numerical instabilities present in the MUSIC algorithm and identify potential causes, with the overall goal of finding new ways to mitigate the instabilities without introducing unphysical elements to the sQGP evolution. The present report presents a review of the hydrodynamic theory applied in MUSIC, a review of the numerical scheme implemented in the algorithm, MUSIC runs demonstrating numerical instabilities, and an instability analysis of the MUSIC sQGP evolution where root causes are identified.

1.2 Hydrodynamic Theory

Theoretical applications of hydrodynamics in high-energy phenomena have been present since L. D. Landau's seminal work [1]. Hydrodynamics presents itself as a useful tool due to it being a coarse grained theory, meaning that it averages out the short-distance and short-time interactions of particles. Essentially, when a system contains too many particles, studying the microscopic details of the system becomes a difficult task. Conversely, when a system contains a sufficient amount of particles, it admits analytical studies by the application of thermodynamic concepts. This application is especially true for systems in static equilibrium, which can be described using few quantities, namely, temperature, collective velocity, and chemical potential. Here, too many particles would refer to a system that, for example, contains a size comparable or greater than 100 particle quantum wavefunctions, which would

require 10^{300} grid points when each axis is discretized with 10 points. Such a system contains too many particles to keep track of individually. On the other hand, if the system is composed of 100 classical particles, that would require keeping track of 600 numbers for the coordinates and momenta, which is feasible. If, however, the system were composed of an Avogadro's number of classical particles, it would become unfeasible to keep track of each one once more.

Now, in the case of sQGP, there is a large number of particles but the system is not in static equilibrium [2]. Nonetheless, the coarse-grained collective motion of the system can be studied by applying the concept of local equilibrium to the system. The concept of local equilibrium demands that the expansion rate of the system be slower than the microscopic interaction rate. The key idea is that the local system of interest must be microscopically large but macroscopically small. This is applied to the sQGP by defining a locally static fluid cell at a time t and position vector $\mathbf{x}$ with thermodynamic properties of temperature $T(t, \mathbf{x})$, chemical potential $\mu_B(t, \mathbf{x})$, and flow velocity $u^\mu(t, \mathbf{x})$. Therefore, only the dynamics of these properties can be studied within this model, and because these properties are essentially the Lagrange multipliers to fix the average energy, momentum, and net charge, the conservation laws can be exploited to study these dynamics.

In hydrodynamics, the equations are based on conservation laws, an equation of state, and a constitutive relationships for dissipative hydrodynamics [2]. In the ideal case, the evolution of the system that is created from the relativistic heavy-ion collisions is described by the conservation laws only,

$$\begin{aligned} \partial_\mu T^{\mu\nu} &= 0 \\ \partial_\mu J^\mu_B &= 0, \end{aligned} \tag{1}$$

where we denote $T^{\mu\nu}$ as the energy-momentum tensor and J^μ_B as the net baryon current, for $\mu = 0, 1, 2, 3$. Then, terms can be re-expressed using timelike flow vector u^μ as,

$$\begin{aligned} T^{\mu\nu}_{\text{ideal}} &= \epsilon u^\mu u^\nu - P\Delta^{\mu\nu} \\ \Delta^{\mu\nu} &= g^{\mu\nu} - u^\mu u^\nu \\ J^\mu_{B,\text{ideal}} &= \rho_B u^\mu \end{aligned} \tag{2}$$

for energy density ϵ, pressure P, baryon density ρ_B, and the metric tensor $g^{\mu\nu} = \text{Diag}(1, -1, -1, -1)$.

Taking this, the system is closed under the equilibrium equation of state of the form

$$P = P(\epsilon, \rho_B), \tag{3}$$

which acts as a constraint on the variables and carries the thermodynamical information of the system. Here closed means the system has an equal number of equations and number of unknowns. Following this setup, the viscous properties of the system are implemented following the Israel-Stewart formalism [3]. This second-order formalism avoids unphysical effects such as the superluminal propagation that occurs in Navier-Stokes form, where the group velocity $\frac{d\omega}{dk}$ for the dispersion relationship $\omega = -Dk^2$ grows in magnitude like k without a bound. The consequence of this is the expression of dissipative hydrodynamics in the form

$$\begin{aligned} T^{\mu\nu} &= T^{\mu\nu}_{\text{ideal}} - \Pi\Delta^{\mu\nu} + \pi^{\mu\nu} \\ J^{\mu}_{B} &= J^{\mu}_{B,\text{ideal}} + V^{\mu}_{B}, \end{aligned} \tag{4}$$

incorporating bulk pressure Π, shear stress tensor $\pi^{\mu\nu}$, and baryon charge diffusion V^{μ}_{B}. In this system, the equations that must be solved are the conservation laws in Eq.(1) and the relaxation equations for dissipative flows [4].

For the purposes of MUSIC, the viscous stress-energy tensor in Eq.(4) is incorporated into the numerical scheme, where a variant of the Israel-Stewart formalism is applied [5]. This form leads to the evolution equations,

$$\partial_\mu T^{\mu\nu} = 0 \tag{5}$$

$$\Delta^{\mu}_{\alpha}\Delta^{\nu}_{\beta}\partial_\sigma \pi^{\alpha\beta} = -\frac{1}{\tau_\pi}(\pi^{\mu\nu} - S^{\mu\nu}) - \frac{4}{3}\pi^{\mu\nu}(\partial_\alpha u^\alpha) \tag{6}$$

$$\partial_\alpha(u^\alpha \Pi) = -\frac{1}{\tau_\Pi}(\Pi + \zeta\theta + \tau_\Pi \Pi\theta/3), \tag{7}$$

where τ_π represents the relaxation time for the shear stress tensor, τ_Π represents the relaxation time for the bulk pressure, ζ represents the bulk viscosity, $\theta = \partial_\alpha u^\alpha$ represents the expansion rate, and $S^{\mu\nu}$ represents the viscous part of the stress-energy tensor in the first order Navier-

Stokes formalism. It has the following form,

$$S^{\mu\nu} = \eta(\nabla^\mu u^\nu + \nabla^\nu u^\mu - \frac{2}{3}\Delta^{\mu\nu}\nabla_\alpha u^\alpha) \tag{8}$$

$$\nabla^\mu = \Delta^{\mu\nu}\partial_\nu, \tag{9}$$

which describes the shear interactions between layers of fluid in terms of shear viscosity η and the velocities of different layers of fluid, with a spatial derivative ∇^μ.

The coordinate system applied in MUSIC is the $\tau - \eta_s$ coordinate system defined by

$$\begin{aligned} t &= \tau\cosh(\eta_s) \\ z &= \tau\sinh(\eta_s), \end{aligned} \tag{10}$$

where τ is the proper time and η_s is the space-time rapidity, and the following evolution equations are obtained, following the indices a, b, c, d for the $\tau - \eta_s$ coordinate system with summations for all dimensions denoted by repeated indices,

$$\begin{aligned} \partial_a T^{ab}_{\text{ideal}} &= \partial_a \pi^{ab} + F^b \\ \partial_a(u^a\pi^{cd}) &= -\frac{1}{\tau_\pi}(\pi^{cd} - S^{cd}) + G^{cd} \end{aligned} \tag{11}$$

where F^b and G^{cd} are the geometrical source terms that are introduced from the coordinate change in Eqs.(10) and the projections in the evolution Eq.(5) and Eq.(6), and τ_π stands for the relaxation time.

To solve these conservation equations, the Kurganov-Tadmor (KT) method is employed [6]; however, in the viscous case, a regulator is used to prevent numerical instabilities from arising.

2 Methodology

2.1 Kurganov-Tadmor Method

The KT method is the algorithm used in MUSIC to solve the equations of hydrodynamics [7]. The KT method is part of the MUSCL family of partial differential equation solver and is effective in the context of hydrodynamics as it is an algorithm designed to deal with large gradients in partial differential equations. As discussed above, hydrodynamic equations stem from conservation laws and possess the general form

$$\partial_t \rho_a = -\nabla \cdot \mathbf{J_a}, \tag{12}$$

for an a from 0 to 4 that denotes energy, three components of the momentum, and the net baryon density. Therefore, the aim of KT is to solve these equations with the equation of state Eq.(3). The KT method can be illustrated through a single component conservation equation in one spatial dimension of the form

$$\partial_t \rho_a = -\partial_x J, \tag{13}$$

provided that there is an equation that links J and ρ, that is, the equation of state. This is because dealing with higher dimensions is simply a matter of applying this same method to all spatial dimensions. All discrete numerical schemes for solving conservation laws contain a numerical viscosity. An advantage of the KT algorithm is that the numerical viscosity term only depends on a positive Δx element, which allows for the transformation of the difference equations resulting from discretization into ordinary differential equations.

The KT is a finite volume method where the cell average of density ρ around position x_j is used rather than the density at the position itself. By averaging over the j-th cell with the boundaries at $x_{j\pm1/2}$, the conservation law becomes,

$$\frac{d}{dt}\bar{\rho}_j(t) = \frac{J(x_{j-1/2}, t) - J(x_{j+1/2}, t)}{\Delta x} \tag{14}$$

and current and charge density at other positions are constructed using a piecewise linear approximation using $\bar{\rho}_j$. Discontinuities arise at the boundary points $x_{j\pm1/2}$ where current evaluations occur; however, this is mitigated by applying the maximum local propagation speed, $a = |\partial J/\partial\rho|$, to evaluate the influence of the discontinuities at this point. The space is then divided into two groups: one that includes the discontinuity elements and another where the solution is smooth.

The KT method provides the following result for the conservation law in the $\Delta t \to 0$ limit:

$$\frac{d}{dt}\bar{\rho}_j(t) = -\frac{H_{j+1/2}(t) - H_{j-1/2}(t)}{\Delta x} \tag{15}$$

such that:

$$H_{j\pm1/2}(t) = \frac{J(x_{j\pm1/2,+}, t) + J(x_{j\pm1/2,-}, t)}{2} - \frac{a_{j\pm1/2}(t)}{2}(\bar{\rho}_{j\pm1/2,+}(t) - \bar{\rho}_{j\pm1/2,-}(t)) \tag{16}$$

where $x_{j\pm1/2,+}$ and $x_{j\pm1/2,-}$ represent the values of the piecewise linear x when approaching $x_{j\pm1/2}$ from the right and left, respectively, and where,

$$\begin{aligned} \bar{\rho}_{j+1/2,+}(t) &= \bar{\rho}_{j+1} - \frac{\Delta x}{2}(\rho_x)_{j+1} \\ \bar{\rho}_{j+1/2,-}(t) &= \bar{\rho}_j + \frac{\Delta x}{2}(\rho_x)_j. \end{aligned} \tag{17}$$

This result provides the numerical scheme to calculate the change in energy in each fluid cell. The algorithm takes into account the average current on each boundary in the first term of Eq.(16) and then accounts for small variations in each band by implementing an average speed of sound term, represented by the second term in Eq.(16).

Here, the order of the spatial derivatives $(\rho_x)_j$ is chosen through a minmod flux limiter such that,

$$(\rho_x)_j = \text{minmod}(\theta\frac{\bar{\rho}_{\text{j+1}} - \bar{\rho}_{\text{j}}}{\Delta\text{x}}, \frac{\bar{\rho}_{\text{j+1}} - \bar{\rho}_{\text{j-1}}}{2\Delta\text{x}}, \theta\frac{\bar{\rho}_{\text{j}} - \bar{\rho}_{\text{j-1}}}{\Delta\text{x}}) \tag{18}$$

such that,

$$\text{minmod}(x_1, \ldots) = \begin{cases} \min\{x_j\} & \text{if } x_j > 0 \,\forall j \\ \max\{x_j\} & \text{if } x_j < 0 \,\forall j \\ 0 & \text{otherwise} \end{cases} \tag{19}$$

where the parameter $\theta = 1.1$ controls the amount of diffusion and oscillatory behaviour for $1 < \theta < 2$. The value of θ was chosen to allow for higher accuracy when dealing with second order approximations whenever possible and preventing oscillations in sections dominated by stiff gradients by opting for first order approximations if needed.

2.2 Numerical Implementation

To implement the KT algorithm in the context of this system, the conservation law $\partial_\mu J^\mu_B = 0$ is represented as

$$\partial_\tau(\tau J^\tau) + \partial_v(\tau J^v) + \partial_{\eta_s} J^{\eta_s} = 0, \tag{20}$$

where

$$\begin{aligned} J^\tau &= \cosh(\eta_s) J^0 - \sinh(\eta_s) J^3 \\ J^\eta &= \cosh(\eta_s) J^3 - \sinh(\eta_s) J^0, \end{aligned} \tag{21}$$

which represents the Lorentz boost with spacetime rapidity $\eta_s = \tanh^{-1}(z/t)$, here the index v denotes the transverse x and y coordinates, which are not affected by the boost like z. The following equations are obtained by applying the same transformation on both indices of $T^{\mu\nu}$,

$$\begin{aligned} &\partial_\tau(\tau T^{\tau\tau}_{\text{ideal}}) + \partial_{\eta_s}(T^{\eta_s\tau}_{\text{ideal}}) + \partial_v(\tau T^{v\tau}_{\text{ideal}}) + T^{\eta_s\eta_s}_{\text{ideal}} \\ &\qquad + \partial_\tau(\tau\pi^{\tau\tau}) + \partial_{\eta_s}(\pi^{\eta_s\tau}) + \partial_v(\tau\pi^{v\tau}) + \pi^{\eta_s\eta_s} = 0 \end{aligned} \tag{22}$$

$$\begin{aligned} &\partial_\tau(\tau T^{\tau\eta_s}_{\text{ideal}}) + \partial_{\eta_s}(T^{\eta_s\eta_s}_{\text{ideal}}) + \partial_v(\tau T^{v\eta_s}_{\text{ideal}}) + T^{\tau\eta_s}_{\text{ideal}} \\ &\qquad + \partial_\tau(\tau\pi^{\tau\eta_s}) + \partial_{\eta_s}(\pi^{\eta_s\eta_s}) + \partial_v(\tau\pi^{v\eta_s}) + \pi^{\tau\eta_s} = 0 \end{aligned} \tag{23}$$

$$\begin{aligned} &\partial_\tau(\tau T^{\tau v}_{\text{ideal}}) + \partial_{\eta_s}(T^{\eta_s v}_{\text{ideal}}) + \partial_w(\tau T^{wv}_{\text{ideal}}) \\ &\qquad + \partial_\tau(\tau\pi^{\tau v}) + \partial_{\eta_s}(\pi^{\eta_s v}) + \partial_w(\tau\pi^{wv}) = 0, \end{aligned} \tag{24}$$

where the indices v and w are for the transverse directions. Hence, there are a total of five equations of interest, the net baryon current in Eq.(20), the energy and momentum in Eqs.(22), (23), and (24), and the viscous part of the stress-energy tensor as $\partial_a(u^a\pi^{cd})$ in Eq.(11). The relaxation equation for the viscous tensor can be written as,

$$\begin{aligned}\partial_c(u^c\pi^{ab}) = &-\frac{1}{2\tau}u^\tau\pi^{ab} + \frac{1}{\tau}\Delta^{a\eta}u^\eta\pi^{b\tau} \\ &-\frac{1}{\tau}\Delta^{a\tau}u^\eta\pi^{b\eta} - g_{cf}\pi^{cb}u^a Du^f - \frac{\pi^{ab}}{2\tau_\pi} \\ &-\frac{1}{6}\pi^{ab}\partial_c u^c + \frac{\eta}{\tau_\pi}(-\frac{1}{\tau}\Delta^{a\eta}g^{b\eta}u^\tau + \frac{1}{\tau}\Delta^{a\eta}g^{b\tau}u^\tau \\ &+ g^{ac}\partial_c u^b - u^a Du^b - \frac{1}{3}\Delta^{ab}\partial_c u^c) + (a \leftrightarrow b)\end{aligned} \tag{25}$$

where the relaxation time τ_π is set to $3\eta/(\epsilon + P)$ [8].

Now, to solve these equations, the KT algorithm is applied along with Heun's method [7]. Heun's method is a form of a second-order Runge-Kutta numerical method and operates by considering an ordinary differential equation of the form

$$\frac{d\rho}{dt} = f(t, \rho), \tag{26}$$

and applying a numerical scheme where

1. Compute $k_1 = f(t, \rho)$
2. Compute $\rho'_{n+1} = \rho_n + k_1\Delta t$
3. Compute $k_2 = f(t + \Delta t, \rho'_{n+1})$
4. Compute $\rho_{n+1} = \rho_n + (k_1 + k_2)\Delta t/2$

So one entire step is comprised of the first step computed with Heun's method for Eqs.(20), (22), (23), and (24), then the first step for Eq.(25), followed by a second step with Eqs.(20), (22), (23), and (24) using the evolved result for π^{ab}, and finally a second step for Eq.(25).

For viscous hydrodynamic evolution, time derivatives appear in the source terms of Eqs.(22), (23), (24), and (25). This is addressed in the algorithm by implementing the

first order approximation,

$$\dot{g}(\tau_n) = (g(\tau_n) - g(\tau_{n-1}))/\Delta\tau, \tag{27}$$

in the first step of Heun's method, and the following approximation in the second step,

$$\dot{g}(\tau_n) = (g^*(\tau_{n+1}) - g(\tau_n))/\Delta\tau, \tag{28}$$

where $g^*(\tau_{n+1})$ is the result given by the first step [8].

This scheme is subject to numerical instabilities during multiple stages of the evolution and at the edges of the system, potentially whenever large gradients occur. The regulator in MUSIC, QuestRevert, regulates instabilities empirically by smoothing out large gradients to ensure that the fluid remains continuous. These instabilities occur primarily in low-density regions, so regularizing is possible as the instabilities do not affect the bulk of the sQGP evolution but there is still a risk of unphysical effects being introduced into the evolution.

3 Results

The MUSIC runs used in this study, shown in Fig.1 and Fig.2, were for lead-lead (Pb-Pb) collisions. The stable run is shown in Fig.1 and depicts the start and end of the evolution for sQGP for MUSIC running as intended, including all safeguards that prevent numerical instabilities from arising, such as QuestRevert. The unstable run is shown in Fig.2 and it depicts the start and end sQGP evolution with all the safeguards rendered ineffective. Particularly, QuestRevert's effect was turned off from all the elements in the MUSIC algorithm.

In the stable case, Fig.1 showcases the expected sQGP evolution, the sQGP expands then cools and the evolution is smooth with no large jumps or gaps at any point. The unstable case in Fig.2 demonstrates unphysical effects due to numerical instabilities arising from eliminating the safeguards in the MUSIC algorithm. This is clear from more pronounced gaps at the edges of the sQGP evolution and inconsistent spots that break the continuity of the hydrodynamic evolution, notably a discontinuous pixel that appears at $(x, y, \tau) = (-2, -5, 1.163)$ and the isolated pixel that appears at $(x, y, \tau) = (10, 0, 3.403)$.

A total of 20 sQGP evolutions were performed to analyze the numerical instabilities

present in MUSIC. The instability analysis described below was applied to all 20 runs. The instabilities present in the runs demonstrate similar behaviour and one of these runs, shown in Fig.3, is described below. The sQGP evolution shown in Fig.3 shows a zoomed in region of a run with numerical instabilities due to QuestRevert being rendered ineffective, covering the area of $x = (0, 15)$ and $y = (-7.5, 7.5)$ to increase the resolution of the instabilities. Numerical instabilities in Fig.3 are present as discontinuities in the sQGP, such as the instabilities that appear in the pixels $(x, y, \tau) = (0, -5, 0.853)$, $(7.5, -4, 0.853)$, $(6, 0, 0.853)$, and $(7.5, 2.5, 1.018)$, as well as the edges of the sQGP as it evolves.

The flow velocity of the instabilities in Fig.3 are analyzed in Fig.4, which examines the region $x = (0, 7.5)$, $y = (-6, 2)$ and shows the flow velocity vectors as green arrows. The unstable regions in Fig.4 demonstrate unphysically large flow velocities, as shown by the vectors with much larger magnitudes that manifest within these regions. The expansion rate is analyzed in Fig.5, which contrasts the temperature values in the top with the expansion rate values in the bottom for the same unstable run shown in Fig.3. Numerically unstable regions plotted with temperature are associated with high values of expansion rate at the instability region or within the surrounding area. Values of the Navier-Stokes tensor are shown in Fig.6 with temperature values shown in the top and Navier-Stokes values shown in the bottom. Navier-Stokes tensor reaches peak values at numerical instabilities and surrounding areas, demonstrating the large unphysical values at unstable regions. The behaviour for flow velocity, expansion rate, and Navier-Stokes tensor described for Fig.3 is consistent with the behaviour of these variables for the other 19 runs performed for this project.

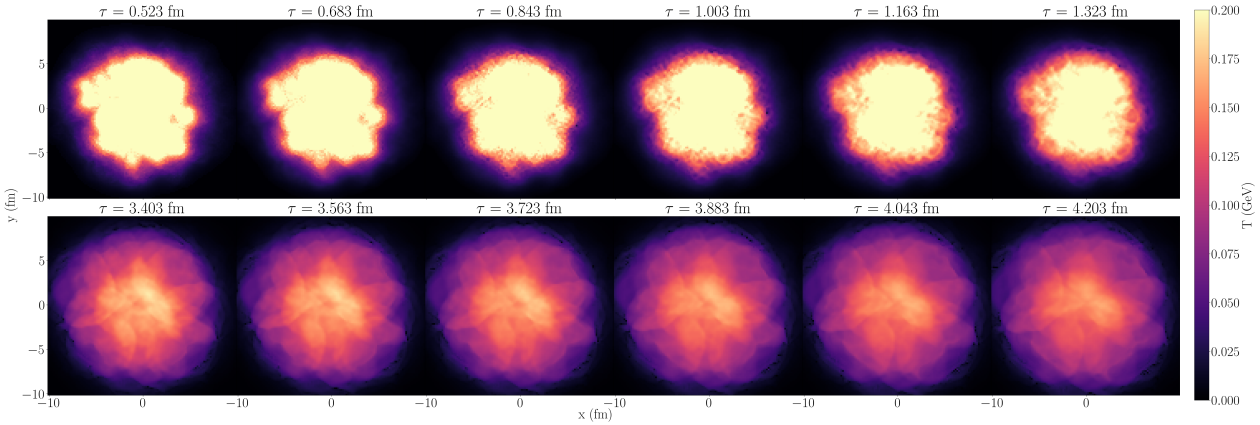

Figure 1: Temperature values for stable MUSIC sQGP evolution for Pb-Pb collision system with IP Glasma initial conditions at energy level $\sqrt{s} = 2.76$ TeV, impact parameter b = 4.5 fm, 0-10% centrality.

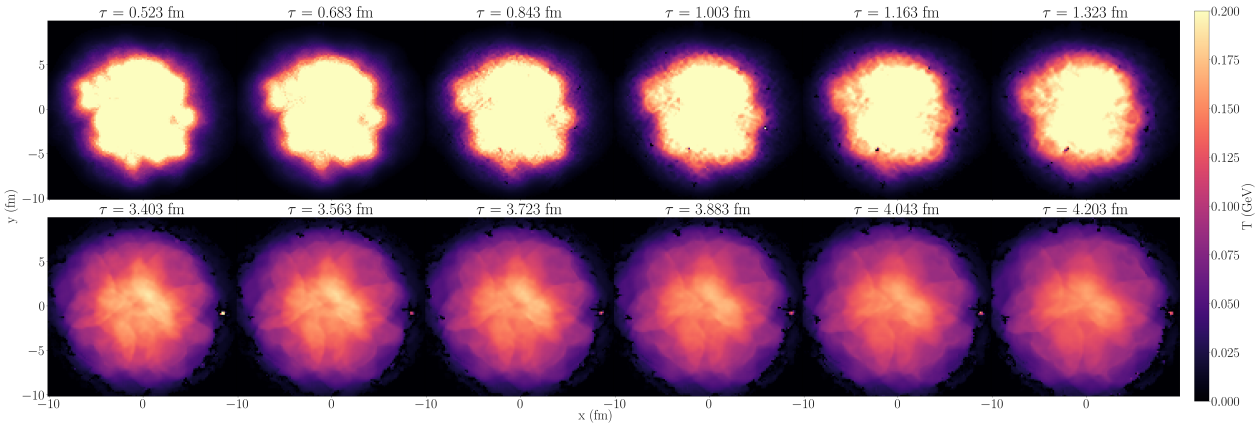

Figure 2: Temperature values for MUSIC sQGP evolution with QuestRevert regulator rendered ineffective for Pb-Pb collision system with IP Glasma initial conditions at energy level $\sqrt{s} = 2.76$ TeV, impact parameter b = 4.5 fm, 0-10% centrality, instability spots appear at the edges and within sQGP evolution.

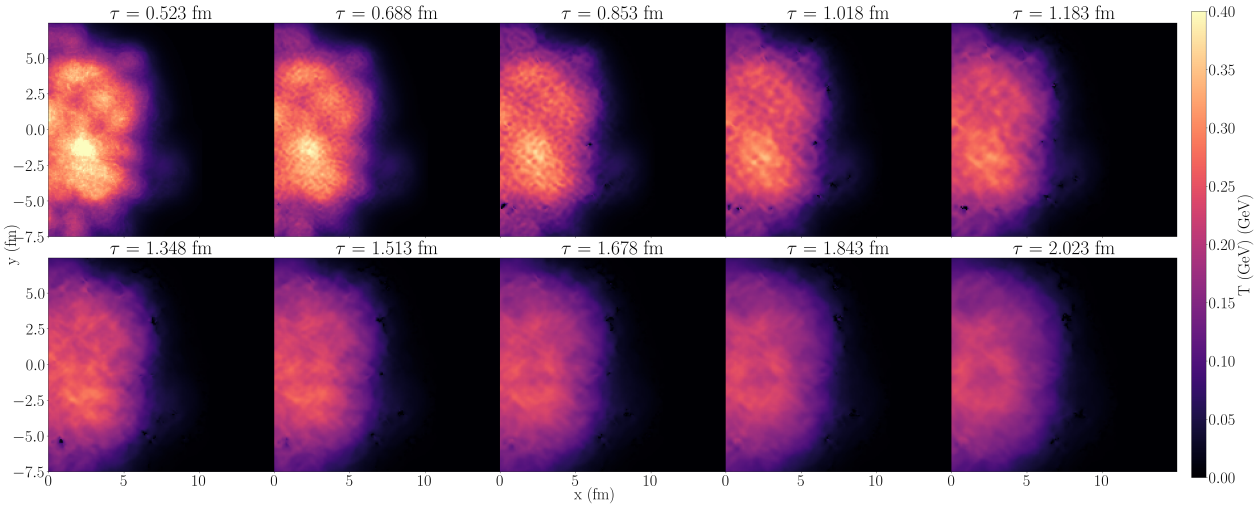

Figure 3: Zoom of region $x = (0, 15)$, $y = (-7.5, 7.5)$ of temperature values of MUSIC sQGP evolution with QuestRevert regulator rendered ineffective for Pb-Pb collision system with IP Glasma initial conditions at energy level $\sqrt{s} = 2.76$ TeV, impact parameter b = 1.65 fm, 0-10% centrality, instability spots appear at the edges and within sQGP evolution.

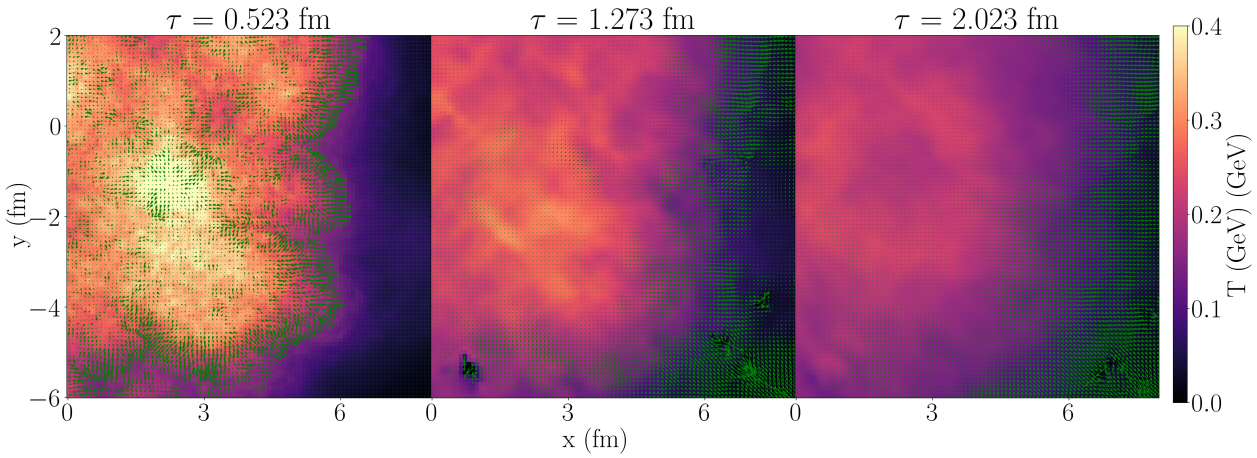

Figure 4: Zoom of region $x = (0, 7.5)$, $y = (-6, 2)$ of temperature values of MUSIC sQGP evolution with QuestRevert regulator rendered ineffective for Pb-Pb collision system with IP Glasma initial conditions at energy level $\sqrt{s} = 2.76$ TeV, impact parameter b = 1.65 fm, 0-10% centrality, flow velocity arrows plotted for each pixel with larger vectors occurring near instabilities.

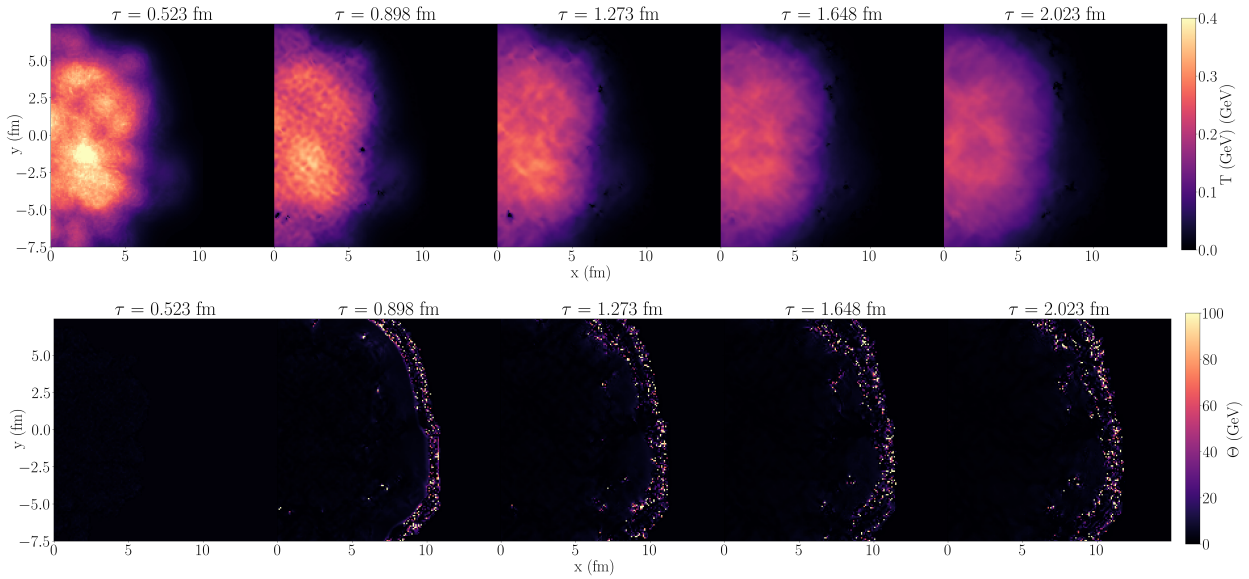

Figure 5: Zoom of region $x = (0, 15)$, $y = (-7.5, 7.5)$ of MUSIC sQGP evolution with ineffective QuestRevert for Pb-Pb collision system with IP Glasma at energy level $\sqrt{s} = 2.76$ TeV, impact parameter b = 1.65 fm, 0-10% centrality, visualized for temperature (top) and expansion rate values (bottom), which light up near instability regions.

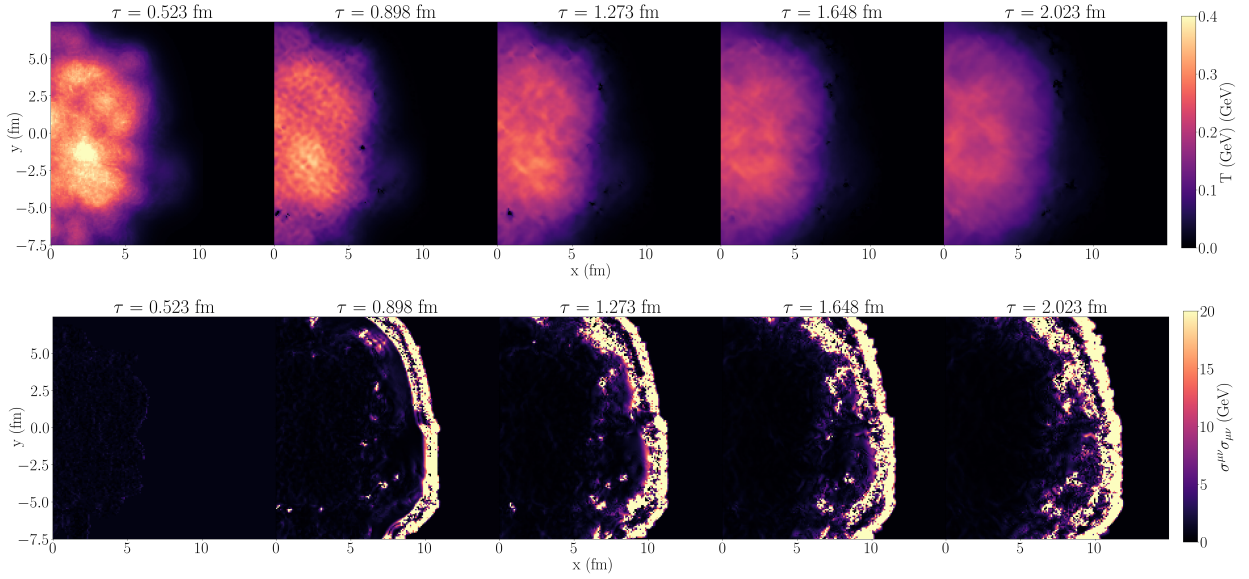

Figure 6: Zoom of region $x = (0, 15)$, $y = (-7.5, 7.5)$ of MUSIC sQGP evolution with ineffective QuestRevert for Pb-Pb collision system with IP Glasma at energy level $\sqrt{s} = 2.76$ TeV, impact parameter b = 1.65 fm, 0-10% centrality, visualized for temperature (top) and Navier-Stokes tensor values (bottom), which peak at instability regions.

4 Discussion

From Fig.1 and Fig.2, this study presents first samples of numerical instabilities in the MUSIC simulation. This instability arises after rendering the regulating code QuestRevert from the MUSIC program ineffective. QuestRevert operates by smoothing out the transitions where there are large spikes in the numerical scheme, such as the regions where there is a sharp transition between matter and vacuum in the sQGP simulation. This process is necessary to ensure that the sQGP evolution has no unphysical elements. In more detail, the numerical instabilities happen at areas of low-density where there should be a small amount of matter, so there should be a minimal effect on the observables. However, if these instabilities are left unchecked the system becomes unphysical. This can be observed from Fig.2, where the observed effect of diminishing the influence of QuestRevert results in large gaps in the edges of the sQGP, which are inconsistent with the continuous evolution of the stable hydrodynamic model in Fig.1. This type of instability is common in hydrodynamic models, as large gradients tend to occur in low-density regions at the boundaries [9,10]. From these results, this report showcases clear instabilities in the MUSIC algorithm.

The instabilities present in the MUSIC algorithm are subjected to a thorough analysis to identify root causes. As unphysically large gradients are suspected to be the root cause for numerical instabilities present in MUSIC, the associated "symptoms" examined in the instability analysis are unphysically large values for the flow velocity, expansion rate, and Navier-Stokes tensor at the unstable regions. To examine these variables, increased resolution is needed, so Fig.3 depicts an unstable sQGP evolution with a zoom into the unstable region in order to obtain a higher resolution for the instability analysis.

Firstly, Fig.4 demonstrates unphysically large flow velocity vectors at unstable regions in the sQGP evolution. This is clear from the plot as the flow velocity vectors, depicted as green arrows for each pixel, demonstrate much larger magnitudes at the instabilities at the bottom left and bottom right of the plot at $(x, y, \tau) = (1, -5, 1.273)$ and $(7, -5, 1.273)$, respectively, as well as for the instability in the bottom right at $(x, y, \tau) = (7, -5, 2.023)$. This demonstrates that there is an association between unphysically large flow velocity vectors and numerical instabilities in MUSIC sQGP evolutions.

Furthermore, expansion rate also demonstrated unphysically large values at unstable regions. Fig.5 shows that the numerical instabilities shown in the evolution plotted for temperature at the bottom left $(x, y, \tau) = (0, -5, 0.898)$ and bottom right $(7.5, -4, 0.898)$ correspond to unphysically large values for the expansion rate at the same regions. The same association is seen with the numerical instability at $(x, y, \tau) = (7.5, 2.5, 1.273)$, which is associated with unphysically large values for the expansion rate at the discontinuity as well as the surrounding area. Therefore, this analysis shows expansion rate exhibits high values in unstable regions.

Moreover, the Navier-Stokes tensor has shown the most unphysical behaviour of the variables presented in this analysis. From Fig.6, the bottom plot showing the values for the Navier-Stokes tensor demonstrates peak values at the instability regions as well as the surrounding areas. This is visible from the the peak values displayed at the instabilities at the bottom left $(x, y, \tau) = (0, -5, 0.898)$ and right $(7.5, -4, 0.898)$ regions in the plot, as well as the discontinuities at $(x, y, \tau) = (7.5, 2.5, 1.273)$ and $(6, 0, 0.898)$ and the surrounding areas. From this then, the Navier-Stokes tensor exhibits the most unphysical behaviour at unstable regions out of the variables presented here.

From the analysis presented above, this study demonstrates that numerical instabilities in MUSIC sQGP evolutions are associated with unphysical effects for the flow velocity, expansion rate, and Navier-Stokes tensor. This is evident from the unphysically large flow velocity vectors and expansion rate values found in unstable regions, as well as the peak values for the Navier-Stokes tensor found at numerical instabilities and surrounding areas, which shows that the Navier-Stokes tensor behaves most unphysically near unstable regions out of the variables analyzed here. This analysis is supported by similar behaviour in other 19 unstable MUSIC sQGP runs. From these behaviours, it is possible to conclude that the root cause for numerical instabilities in MUSIC is unphysically large gradients occurring at low-density regions.

5 Conclusion

This report first sought to introduce the theoretical and computational framework for this honours research thesis. From this introduction, we present samples of numerical instability present in the MUSIC simulation and identify unphysically large values for flow velocity, expansion rate, and the Navier-Stokes tensor at the unstable regions, which are the consequence of unphysically large gradients occuring at low density regions in the sQGP evolution. Therefore, this study successfully demonstrates that unphysically large gradients in regions of low density are the root cause for instabilities seen in MUSIC sQGP evolutions. Future steps in this work will be comprised of investigating new techniques to mitigate numerical instabilities in MUSIC without introducing unphysical effects in the sQGP evolutions.

References

[1] L. Landau, Izv. Akad. Nauk Ser. Fiz **17**, 51-64 (1953). 1

[2] S. Jeon and U. Heinz, International Journal of Modern Physics E **24**, 10, 1530010 (2015). 2

[3] W. Israel and J. M. Stewart, Annals of Physics **118**, 2, 341-372 (1979). 3

[4] A. S. Khvorostukhin, E. E. Kolomeitsev, and V. D. Toneev, arXiv:1810.10303 (2018). 3

[5] B. Schenke, S. Jeon, and C. Gale, Physical Review Letters **106**, 4, 042301 (2011). 3

[6] A. Kurganov and E. Tadmor, Journal of Computational Physics **160**, 1, 241-282 (2000). 4

[7] B. Schenke, S. Jeon, and C. Gale, Physical Review C **82**, 1, 014903 (2010). 5, 8

[8] B. Schenke, S. Jeon, and C. Gale, Physical Review C **85**, 2, 024901 (2012). 8, 9

[9] M. Duez *et al.*, Physical Review D **67**, 2, 024004 (2003). 14

[10] M. Duez *et al.*, Physical Review D **69**, 10, 104030 (2004). 14